Journal of Nonlinear Science (2026) 36:86
https://doi.org/10.1007/s00332-026-10302-7

Journal of Nonlinear Science

Pattern Formation from Nonlocal Conflict Memory in a PDE-ODE Model

Shu Li[1] · **Binxiang Dai**[1,3] · **Hao Wang**[2]

Received: 19 November 2025 / Accepted: 23 June 2026

Abstract

Many territorial animals shape their movement decisions using memory of past conflicts, yet the population-level consequences of such nonlocal conflict memory remain poorly understood. We propose and analyze a PDE-ODE hybrid model for a single population moving in response to spatial memory of territorial conflicts. The population density satisfies a diffusion equation with delayed, nonlocal advection generated by a convolution of a conflict variable, while the conflict intensity evolves according to a local ODE encoding a warning mechanism with decay and resetting. Linearization about the positive homogeneous steady state yields a non-self-adjoint operator whose spectrum reduces to a countable family of characteristic equations indexed by Fourier modes. For Gaussian and Laplacian perception kernels, the steady state is linearly asymptotically stable for all perceptual radii in the memoryless case, whereas a top-hat kernel admits diffusion-driven (Turing) instability below a critical radius, producing stationary spatial patterns. For positive memory delay, we identify Hopf bifurcation thresholds at the level of the linearized spectral problem for all three kernels. In the top-hat case, the stationary and oscillatory thresholds may meet in the (R, τ)-plane, giving a codimension-two Turing-Hopf spectral point. Numerical simulations illustrate these thresholds and the associated spatial and spatiotemporal patterns.

Communicated by Nikolaos Sfakianakis.

✉ Binxiang Dai
bxdai@csu.edu.cn

✉ Hao Wang
hao8@ualberta.ca

Shu Li
shli97@csu.edu.cn

1 School of Mathematics and Statistics, HNP-LAMA, Central South University, Changsha, Hunan 410083, People's Republic of China

2 Department of Mathematical and Statistical Sciences, University of Alberta, Edmonton, AB T6G 2G1, Canada

3 Hunan University of Information Technology, Changsha, Hunan 410151, China

Published online: 16 July 2026

Keywords PDE-ODE coupled model · Nonlocal memory · Warning mechanisms · Spatiotemporal dynamics · Turing instability · Hopf crossing

1 Introduction

Since Turing's seminal work (Turing 1990), diffusion-driven instability has been regarded as a fundamental mechanism for spatial pattern formation in biological systems. Traditional reaction–diffusion models assume that individuals move randomly and interact only locally. However, animal movement is a complex cognitive process rather than a purely physical one. Numerous empirical studies have shown that animals use past experiences and environmental cues to make movement decisions that improve their chances of survival and reproduction. Cognitive processes play a significant role in shaping these decisions, and different cognitive mechanisms can result in remarkably diverse spatial patterns of space use (Fagan et al. 2013; Golledge 1999; O'Keefe and Nadel 1978). Although the specific neurological and behavioral mechanisms remain under debate, most researchers agree that perception, which means acquiring information about the environment, and memory, which is the storage, encoding, and recalling of that information, are dominant drivers of animal movement behaviors. Recently, Wang and Salmaniw (2023) integrated cognition into animal movement and proposed the following reaction–diffusion–advection equation:

$$\frac{\partial u}{\partial t}(x,t) = \underbrace{d_1 \triangle u(x,t)}_{\text{Diffusive movement}} + \underbrace{d_2 \nabla \cdot (u \nabla a(x,t))}_{\text{Cognitive advection}} + f(u), \quad x \in \Omega, t > 0, \tag{1}$$

where the advective potential $a(x,t)$ can be considered as the attractivity of a point at a given time, and then, we can describe different forms of cognitive behavior by giving different forms of $a(x,t)$. Xue et al. (2024) considered a kind of nonlocal memory as $a(x,t) = K * u(x,t-\tau) = \int_\Omega K(x-y)u(y,t-\tau)\mathrm{d}y$ and investigated the following model:

$$\frac{\partial u}{\partial t}(x,t) = d_1 \triangle u(x,t) + d_2 \nabla \cdot (u(x,t) \nabla (K * u)(x,t-\tau)) + f(u(x,t)), \tag{2}$$

where the spatial kernel function $K(x-y)$ is chosen for the Top-hat kernel function under the periodic boundary conditions. They demonstrated that the joint effects of the memory delay τ and the perceptual radius R can generate richer spatiotemporal dynamics than before, including Turing instability, Hopf crossing, and even Turing-Hopf bifurcation. That is quite different from the dynamics of models with discrete memory as $K(x-y) = \delta(x-y)$. Shi et al. (2020) first investigated the reaction–diffusion model with discrete memory and found that the stability of a spatially homogeneous steady state depends entirely on the relationship between the two diffusion coefficients but is independent of the memory delay. They suggested three directions for further exploration of cognitive mechanisms in animal movement. First, one can investigate how the interaction between memory and different forms of reaction kinetics produces more complex dynamical behaviors (An et al. 2020; Shi et al. 2019; Song et al. 2019;

Zhang et al. 2023). Second, the studies of memory effects in two-species systems can reveal how memory influences predation or competition dynamics, which has been conducted extensively, such as Li et al. (2022, 2024); Liu and Jiang (2024); Liu et al. (2023); Shi et al. (2021); Zhang et al. (2024) and therein. Third, it remains a challenging and fundamental problem to determine how different cognitive mechanisms affect the stability and bifurcation of system solutions and to accurately characterize the diversity of animal cognition within mathematical frameworks. Although some researchers have examined the effects of spatiotemporal memory (Li et al. 2025; Liu et al. 2025; Shi et al. 2021) or distributed memory (Li et al. 2025; Shen et al. 2023; Shi and Shi 2024) under different boundary conditions, a common feature of all these models is that the memory process refers only to an individual's own past state or the density of interacting species. This neglects the role of environmental information and animal-environment interactions in shaping the cognitive map that guides movement decisions.

Territorial conflicts occur in many different animal species, from birds to primates, insects to reptiles. While some conflicts manifest as direct physical aggression, such as fights among monkeys or human warfare, many species adopt ritualized aggression to avoid costly injuries. This includes dominance displays, vocalizations, or territorial markings, as observed in birds, bees, and other species. Regardless of whether interactions are violent or ritualized, the ultimate goal of territorial conflicts is to establish and defend space for exclusive use by a particular group, such as a pack, flock, or mating pair. Potts and Lewis (2016) proposed an ODE to describe the cognitive map of conflict zones as follows:

$$\frac{\partial w_i}{\partial t}(x,t) = \Sigma_{j\neq i} p_{ij} u_i u_j - (\mu_i + \beta_i u_i) w_i, \tag{3}$$

where $w_i = w_i(x,t)$ describes the species u_i' spatial cognitive map of conflict zones. p_{ij} represents the extent to which encounters between species u_i and u_j cause the conflict zone to increase, μ_i is the conflict zone decay rate, and β_i is the rate at which the conflict zone decays due to agents revisiting the site and experiencing no conflict. Recently, Liu et al. studied the Turing crossings of a single population model based on (3). Shi et al. (2024) studied a consumer-resource model, where consumers have the learning mechanisms described by the local perception of a cognitive map based on the learning and memory waning.

In many species, individuals do not rely solely on immediate sensory cues when navigating territorial landscapes but instead use memory of past conflicts to inform movement decisions. This cognitive mapping of high-risk areas influences how animals distribute themselves spatially, affecting both individual movement strategies and population-level patterns. To capture this behavior, we introduce conflict zones into system (2), where animals modify their movement in response to past aggressive interactions. By incorporating nonlocal memory and perception, our framework allows individuals to navigate their environment based on past experiences rather than just local density cues. Moreover, such memory of conflict experiences often gives rise to a warning mechanism, through which animals can anticipate potential dangers and adjust their movement before direct encounters occur. In this sense, the cognitive map

functions not only as a record of past events but also as a predictive tool that enables proactive avoidance of high-risk regions. Motivated by the research (Xue et al. 2024; Potts and Lewis 2016), and Wang and Salmaniw (2023), we consider the following PDE-ODE model with a warning mechanism in this paper:

$$\begin{cases} u_t = d_1 u_{xx} + d_2(u(K * w(x, t-\tau))_x)_x + f(u), & x \in \Omega, t > 0, \\ w_t = pu^2 - (\mu + \beta u)w, & x \in \Omega, t > 0, \end{cases} \tag{4}$$

where $d_1 > 0$ is the random diffusion coefficient of u, and $d_2 \geq 0$ is the cognitive advection coefficient of u. We denote that $\Omega = (-L, L)$, $L > 0$ is the spatial domain, and consider the model (4) in a periodic interval Ω with the following periodic boundary conditions:

$$u(-L, t) = u(L, t), \quad u_x(-L, t) = u_x(L, t), \quad t > 0. \tag{5}$$

Assume that there exists a constant $u_* > 0$, such that $f(u_*) = 0$. Then, system (4) has a positive constant steady-state solution (u_*, w_*), where $w_* = \dfrac{pu_*^2}{\mu + \beta u_*}$. Denote $\mathbb{N}_0 = \mathbb{N} \cup \{0\}$, we consider the eigenvalue problem of $-\frac{\partial^2}{\partial x^2}$ with periodic boundary conditions:

$$\begin{cases} -\psi_{xx}(x) = l\psi(x), & x \in (-L, L), \\ \psi_x(-L) = \psi_x(L), \psi(-L) = \psi(L), \end{cases} \tag{6}$$

which has eigenvalues $l_{\pm n} = (\dfrac{n\pi}{L})^2$ and corresponding eigenfunctions

$$\psi_{\pm n}(x) = e^{\pm \frac{in\pi}{L}x} = cos\left(\frac{n\pi}{L}x\right) \pm isin\left(\frac{n\pi}{L}x\right), \tag{7}$$

for $n \in \mathbb{N}_0$. Let

$$c_n(h) = \langle h, \psi_n \rangle = \frac{1}{2L}\int_{-L}^{L} h(x)\psi_{-n}(x)\mathrm{d}x, \tag{8}$$

then we define the linear spaces

$$L^2_{per}(-L, L) = \left\{ h \in L^2(-L, L) : h = \sum_{n=-\infty}^{\infty} c_n(h)\psi_n \text{with} \sum_{n=-\infty}^{\infty} |c_n|^2 < \infty \right\},$$

and

$$H^2_{per}(-L, L) = \left\{ h \in L^2_{per}(-L, L) : h'' \in L^2_{per}(-L, L) \right\}.$$

Suppose that the spatial kernel K satisfies

($\mathbf{H_0}$) $K \in L^1_{per}(-L, L)$, $K(-x) = K(x) \geq 0$ for all $x \in (-L, L)$ and $\int_{-L}^{L} K(y)\mathrm{d}y = 1$, and $K \not\equiv 0$.

The common forms of the detection function K include the Gaussian detection function, the exponential detection function, or the top-hat detection function in the one-dimensional spatial domain $\Omega = \mathbb{R}$ with the following forms:

$$\begin{aligned}
&\text{Gaussian}: \quad K(x) := \frac{1}{\sqrt{2\pi}R} e^{-x^2/2R^2} \\
&\text{Laplacian}: \quad K(x) := \frac{1}{2R} e^{-|x|/R} \\
&\text{Top-hat}: \quad K(x) := \begin{cases} \dfrac{1}{2R}, & -R \le x \le R, \\ 0, & otherwise. \end{cases}
\end{aligned} \tag{9}$$

Here, $R \ge 0$ is the perceptual radius, which is proportional to the standard deviation of the detection function and describes the maximum distance at which landscape features can be distinguished Fagan et al. (2017). The first two functions are Gaussian and Laplacian detection functions, which allow agents to perceive nearby information most clearly and monotonically decay as the distance from the observation location increases. The last function, which we call the Top-hat detection function, imposes strict constraints on the range of information that organisms can detect.

In model (4), it is highly challenging since the system couples a PDE with a nonlinear ODE through a nonlocal, nonlinear, and non-self-adjoint diffusion operator, whose hybrid structure leads to a complicated spectral problem. Through detailed spectral analysis of the linearized operator, we found that it is a point spectrum, which means that the stability of the steady state (u_*, w_*) is determined by analyzing the distribution of characteristic roots of the corresponding eigenvalue problem. It is worth noting that various parameters, including d_1, d_2, τ, R, p, μ, and β, have different effects on the stability and bifurcation of the positive steady state (u_*, w_*); the main results are as follows:

- Whether the perception function is Gaussian, Laplacian, or Top-hat, there exists a constant $S(p, \mu, \beta) > 0$, such that when $\dfrac{d_2}{d_1} \le S$, the positive steady state (u_*, w_*) is linearly asymptotically stable for all $R \ge 0$ and $\tau \ge 0$. (cf. Theorem 4.3, Theorem 4.7)
- In the case of the Gaussian or Laplacian kernel function, when $\dfrac{d_2}{d_1} > S$, there is a threshold $R_H > 0$, such that when $R \ge R_H$, (u_*, w_*) is linearly asymptotically stable for any $\tau \ge 0$; When $0 < R < R_H$, there exists a critical value τ_G^*, such that (u_*, w_*) is linearly asymptotically stable for $\tau \in [0, \tau_G^*)$, (u_*, w_*) is unstable for any $\tau \in (\tau_G^*, +\infty)$, and the characteristic equation has a Hopf crossing at $\tau = \tau_G^*$. (cf. Theorem 4.3, see Fig. 1(Left))
- The case of the Top-hat kernel function is more complex. (cf. Theorem 4.7, see Fig. 1(Right))
  - If $S < \dfrac{d_2}{d_1} < -\dfrac{S}{z_1}$, there exists a threshold $R_*^H > 0$, such that when $R \ge R_*^H$, (u_*, w_*) is linearly asymptotically stable for $\tau \ge 0$; When $0 < R < R_*^H$, there

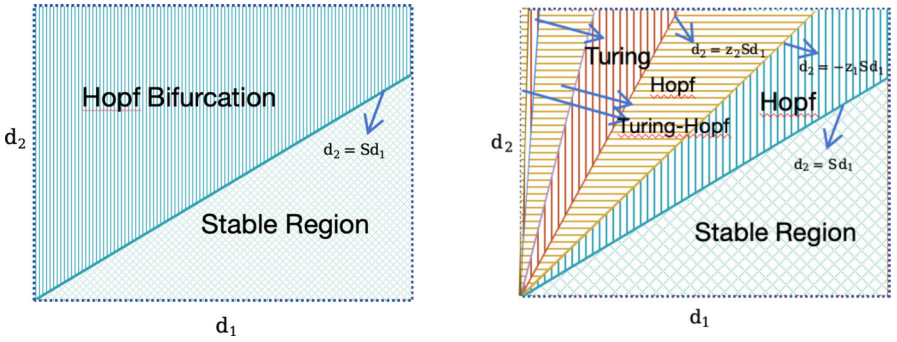

Fig. 1 The local dynamics of (4) at (u_*, w_*) in (d_1, d_2) plane. Left: Gaussian or Laplacian kernel; Right: Top-hat kernel

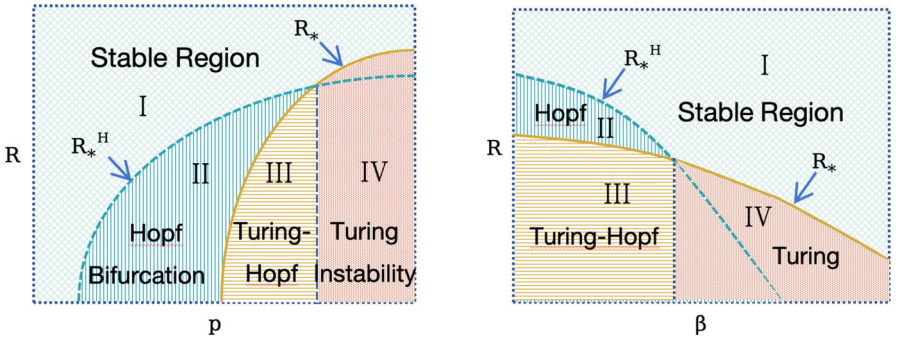

Fig. 2 The local dynamics of (4) with Top-hat kernel at (u_*, w_*) in (p, R) (Left) and (β, R) plane (right)

exists a critical value τ_*, such that (u_*, w_*) is unstable for $\tau \in (\tau_*, +\infty)$ and linearly asymptotically stable for $\tau \in [0, \tau_*)$, and the characteristic equation has a Hopf crossing at $\tau = \tau_*$.

- If $-\frac{S}{z_{2m-1}} < \frac{d_2}{d_1} \leq \frac{S}{z_{2m}}$, $(m = 1, 2, \dots)$, there exists a $R_* < R_*^H$, such that when $R \geq R_*^H$, (u_*, w_*) is linearly asymptotically stable; When $R_* < R < R_*^H$, (u_*, w_*) is unstable for $\tau \in (\tau_*, +\infty)$ and linearly asymptotically stable for $\tau \in [0, \tau_*)$, the system (4) has a Hopf crossing at $\tau = \tau_*$; When $0 < R < R_*$, (u_*, w_*) is unstable for $\tau \geq 0$. Moreover, the system has a Turing-Hopf spectral point $(R, \tau) = (R_*, \tau_*)$.
- If $\frac{S}{z_{2m}} < \frac{d_2}{d_1} \leq -\frac{S}{z_{2m+1}}$, $(m = 1, 2, \dots)$, there is $R_*^H < R_*$, such that when $R > R_*$, (u_*, w_*) is linearly asymptotically stable for $\tau \geq 0$; When $0 < R < R_*$, (u_*, w_*) is unstable for $\tau \geq 0$. The system (4) has a stationary Turing crossing at $R = R_*$ (Fig. 2).

- As p increases, the stability region becomes smaller, implying that frequent or intense territorial conflicts make populations more susceptible to pattern formation or oscillatory dynamics. In contrast, larger values of μ or β, representing

faster memory decay and conflict resetting, enlarge the stability region. Biologically, this suggests that the ability to forget past conflicts or reset warning signals promotes more harmonious and stable coexistence, as excessive persistence of hostility destabilizes population structure and leads to recurrent spatial or temporal fluctuations.

Our study systematically investigates the effects of perceptual radius R and memory delay τ on system dynamics. When memory effects are absent ($\tau = 0$), we find that perception modeled by Gaussian and Laplacian kernels leads to linear asymptotic stability of the steady state for all R, whereas the Top-hat kernel induces Turing instability, leading to self-organized spatial patterns for small R. This suggests that species with sharply localized perception are more likely to exhibit spatially heterogeneous distributions, while those with more diffuse perception remain evenly distributed. When memory effects are included ($\tau > 0$), our spectral analysis shows that Hopf crossings can occur in the parameter regimes identified below. The associated oscillatory dynamics are illustrated by numerical simulations. Furthermore, in the Top-hat kernel case, an additional Turing-Hopf scenario may occur when the Turing threshold and a Hopf threshold meet in the (R, τ)-plane. These findings reveal the interplay between nonlocal perception, spatial memory, and cognitive mapping, and the present work focuses on the linear stability and formal bifurcation thresholds of the spatially homogeneous steady state. A complete well-posedness theory for the PDE-ODE system (4), including existence, uniqueness, and regularity, is not established here. Therefore, the stability and bifurcation statements below should be understood in terms of the linearized spectral problem of the nonlinear model.

The structure of this paper is as follows: In Sect. 2, we study the spectral properties of the linear operator at the positive steady state to ensure that the stability of the positive steady state is determined by the eigenvalues of the characteristic equation. In Sect. 3, we consider the memoryless case, i.e., $\tau = 0$, and study the influence of the animal's perceptual radius R on the stability of (4) and the existence of Turing instability for three different perception kernels, such as Gaussian, Laplacian, and Top-hat kernels. Then, we investigate the influence of memory delay $\tau > 0$ on the Hopf crossing of (4) for the above three different perception kernels and the joint effect of R and τ on the Turing-Hopf spectral interaction for the Top-hat case in Sect. 4. Finally, Sect. 5 presents numerical simulations illustrating the thresholds obtained from the spectral analysis.

2 Spectral Analysis

In order to investigate the stability of the positive constant steady-state solution (u_*, w_*), the linearized Eq. of (4) at the positive steady-state solution (u_*, w_*) is

$$\begin{cases} u_t = d_1 u_{xx} + d_2 u_* (K * w_\tau)_{xx} + f_{u_*} u, & x \in (-L, L), t > 0, \\ w_t = Mu + Nw, & x \in (-L, L), t > 0, \\ u(-L, t) = u(L, t), \quad u_x(-L, t) = u_x(L, t), & t > 0, \end{cases} \tag{10}$$

where

$$M = 2pu_* - \beta w_* = \frac{2p\mu u_* + p\beta u_*^2}{\mu + \beta u_*} > 0, \quad N = -(\mu + \beta u_*) < 0. \tag{11}$$

We denote a space $C_L = C\left([-\tau, 0], L^2_{\text{per}}(-L, L; \mathbb{C})^2\right)$. Then we rewrite (4) as:

$$\frac{\mathrm{d}\Phi}{\mathrm{d}t} = \mathcal{L}\Phi,$$

where $\Phi(\theta) = (\phi(\theta), \varphi(\theta))^T \in C_L$ and

$$\mathcal{L}\Phi(\theta) = \begin{cases} \mathcal{L}_*\Phi + \mathcal{L}_0\Phi(0), & \theta = 0, \\ \dot{\Phi}(\theta), & -\tau \le \theta < 0, \end{cases} \tag{12}$$

with

$$\mathcal{L}_*\Phi = \mathcal{L}_*\begin{pmatrix} \phi \\ \varphi \end{pmatrix} = \begin{pmatrix} d_1\phi_{xx}(0) + d_2u_*(K * \varphi(-\tau))_{xx} \\ 0 \end{pmatrix}. \tag{13}$$

and

$$\mathcal{L}_0 = \begin{pmatrix} f_{u_*} & 0 \\ M & N \end{pmatrix}. \tag{14}$$

The domain of $\mathcal{L}$ is

$$\mathrm{Dom}(\mathcal{L}) = \{\dot{\Phi} \in C_L : \Phi \in \mathrm{Dom}(\mathcal{L}_*), \dot{\Phi}(0) = \mathcal{L}_*\Phi + \mathcal{L}_0\Phi(0)\}$$

where $\mathrm{Dom}(\mathcal{L}_*) = C^2([-\tau, 0], H^2_{per}(-L, L); \mathbb{C}) \subset C_L$,

For the kernel function K, we denote the Fourier coefficient $H(n, R)$ for any $n \in \mathbb{N}$ as follows:

$$H(n, R) = \int_{-L}^{L} e^{-\frac{in\pi y}{L}} K(y)dy = \int_{-L}^{L} cos\left(\frac{n\pi}{L}y\right) K(y)\mathrm{d}y, \tag{15}$$

To show the composition of the spectral set of $\mathcal{L}$, we need to give two Lemmas. It follows from Liu et al. (2025) that K has some properties.

Lemma 2.1 *Assume K satisfies ($\mathbf{H}_0$), and $\psi \in H^2_{per}(-L, L)$, then*

$$(K * \psi)_{xx} = K * (\psi_{xx}), \tag{16}$$

and

$$K * \psi_n = H(n, R)\psi_n, \quad K * \psi_{-n} = H(n, R)\psi_{-n}, \tag{17}$$

where ψ_n, ψ_{-n} are defined in (7), and $H(n, R)$ is defined in (15).

Then, we define the linear operator $\mathcal{A} : D(\mathcal{A} \subset L^2_{per}(-L, L) \to L^2_{per}(-L, L))$ as follows:

$$\begin{cases} D(\mathcal{A}) = H^2_{per}(-L, L), \\ \mathcal{A}\phi = \epsilon\phi_{xx} + \varepsilon K * (\phi_{xx}). \end{cases} \tag{18}$$

Denote $\sigma(\mathcal{A})$ as the spectrum of the linear operator $\mathcal{A}$. Similar to the proof of Proposition 2.1 of Ducrot et al. (2018), the following result for $\sigma(\mathcal{A})$ is obtained.

Lemma 2.2 *The spectrum $\sigma(\mathcal{A})$ is consisted in point spectrum, and one has*

$$\sigma(\mathcal{A}) = \{\nu_n = \nu_{-n} := -l_n[\epsilon + \varepsilon H(n, R)], n \in \mathbb{N}_0\},$$

and the corresponding eigenfunction are $\psi_n(x)$ and $\psi_{-n}(x)$ giving by $\mathcal{A}\psi_n = \lambda\psi_n$, where ϵ and ε are both constants, l_n, $\psi_{\pm n}$ are defined in (7).

Now, we can describe the spectrum of the linear operator $\mathcal{L}$.

Theorem 2.3 *For the linear operator $\mathcal{L}$ defined in (12), the spectrum $\sigma(\mathcal{L})$ of $\mathcal{L}$ only consists of the point spectrum $\sigma_p(\mathcal{L})$ with*

$$\sigma(\mathcal{L}) = \sigma_p(\mathcal{L}) = \{\lambda_n : E(n, \tau, \lambda) = 0, n \in \mathbb{Z}\} \cup \{N\}, \tag{19}$$

where

$$E(n, \tau, \lambda) = \lambda^2 + B_n\lambda + P_n + Q_n e^{-\lambda\tau} = 0, \tag{20}$$

and

$$B_n = d_1 l_n - N - f_{u_*}, \quad P_n = f_{u_*}N - d_1 N l_n, \quad Q_n = d_2 u_* M H(n, R) l_n. \tag{21}$$

Proof Assume that there exists $\Phi(\theta) = (\phi(\theta), \varphi(\theta))^T \in \mathrm{Dom}(\mathcal{L})$, such that

$$(\lambda I_2 - \mathcal{L})\Phi(\theta) = g(\theta), \tag{22}$$

where $\lambda \in \mathbb{C}$, $g(\theta) = (g_1(\theta), g_2(\theta))^T \in \mathrm{Dom}(\mathcal{L}_*)$, and I_2 is a 2D identity matrix. Since for $\theta \in [-\tau, 0)$, there is $\mathcal{L}\Phi(\theta) = \dot{\Phi}(\theta)$ from (12), then (22) could be rewritten as the following linear differential equation:

$$\dot{\Phi}(\theta) = \lambda\Phi(\theta) + g(\theta), \quad \theta \in [-\tau, 0). \tag{23}$$

It is clear that (23) can be solved to the following form:

$$\Phi(\theta) = e^{\lambda\theta}\Phi(0) + \int_0^\theta e^{\lambda(\theta-\xi)} g(\xi)\mathrm{d}\xi, \tag{24}$$

where the initial value $\Phi(0) = (\phi(0), \varphi(0))^T \in H^2_{per}(-L, L) \times H^2_{per}(-L, L)$ satisfies:

$$\dot{\Phi}(0) = \mathcal{L}_*\Phi + \mathcal{L}_0\Phi(0), \tag{25}$$

It follows from (24) that

$$\dot{\Phi}(0) = \lambda\Phi(0) + g(0). \tag{26}$$

Combining (25), (26), (13) and (14), we obtain the following equations:

$$\begin{cases} d_1(\phi(0))_{xx} + d_2u_*(K * \varphi(-\tau))_{xx} + f_{u_*}\phi(0) = \lambda\phi(0) + g_1(0), \\ M\phi(0) + N\varphi(0) = \lambda\varphi(0) + g_2(0), \\ \Phi(-L) = \Phi(L),\ \Phi_x(-L) = \Phi_x(L). \end{cases} \tag{27}$$

For $g(\theta) = 0$, if $\lambda \neq N$, then the second Eq. of (27) can be solved to

$$\varphi(0) = \frac{M\phi(0)}{\lambda - N}. \tag{28}$$

It follows from (24) and (28) that

$$\varphi(-\tau) = \frac{M\phi(0)}{\lambda - N}e^{-\lambda\tau}, \tag{29}$$

substituting (29) into the first Eq. of (27), and combining Lemma (2.1) yields

$$\begin{aligned} 0 =& d_1(\phi(0))_{xx} + d_2u_*e^{-\lambda\tau}(K * (\frac{M\phi(0)}{\lambda - N}))_{xx} + (f_{u_*} - \lambda)\phi(0) \\ =& d_1(\phi(0))_{xx} + d_2u_*e^{-\lambda\tau}\frac{M}{\lambda - N}(K * (\phi(0))_{xx}) + (f_{u_*} - \lambda)\phi(0). \end{aligned} \tag{30}$$

Define a linear operator:

$$\mathcal{D}\phi(0) := d_1(\phi(0))_{xx} + d_2u_*e^{-\lambda\tau}\frac{M}{\lambda - N}(K * (\phi(0))_{xx}), \tag{31}$$

it follows from Lemma (2.2) and (18) that $\Phi(0) = (\phi(0), \varphi(0))^T = (\psi_n, \psi_n)^T$ satisfies (25), where ψ_n is defined in (7), and then, (30) has nonzero solutions if and only if

$$(f_{u_*} - \lambda) \notin \sigma(\mathcal{D}), \tag{32}$$

which implies that

$$\frac{(f_{u_*} - \lambda)(\lambda - N)}{d_1(\lambda - N) + d_2u_*MH(n, R)} \notin \{l_n\}_{n\in\mathbb{N}_0}. \tag{33}$$

That is, the eigenvalue λ satisfies the characteristic Eq. (20). Moreover, the operator $(\lambda I_2 - \mathcal{L})$ has a bounded inverse $(\lambda I_2 - \mathcal{L})^{-1}$ when (33) holds.

If $\lambda = N$, let $g(\theta) = 0$, we consider equations $\mathcal{L}_*\Phi + \mathcal{L}_0\Phi(0) = \lambda\Phi(0)$, i.e.,

$$\begin{cases} d_1(\phi(0))_{xx} + d_2u_*(K * \varphi(-\tau))_{xx} + f_{u_*}\phi(0) = N\phi(0), \\ M\phi(0) = 0, \\ \Phi(-L) = \Phi(L),\ \Phi_x(-L) = \Phi_x(L). \end{cases} \tag{34}$$

It follows from the second Eq. of (34) that $\phi(0) = 0$, combining (24) and the first Eq. of (34) gives that $K * (\psi(0))_{xx} = 0$, which implies that there exists nonzero solutions of (34). Hence, N is also an eigenvalue of $\mathcal{L}$.

For $g(\theta) \neq 0$, let $q(\theta) = \int_0^\theta e^{-\lambda(\theta-\xi)} g_2(\xi) \mathrm{d}\xi$ with $q(0) = 0$. It follows from (16) and (17) that

$$(K * q(-\tau))_{xx} = K * (q(-\tau))_{xx} = \Sigma_{n\in\mathbb{Z}} c_n(q(-\tau)) H(n, R)\psi_n. \tag{35}$$

Then, we focus on Eq. (27) again; the second Eq. of (27) leads to

$$\varphi(0) = \frac{M\phi(0) - g_2(0)}{\lambda - N}, \tag{36}$$

combining (24) and (36), we have

$$\varphi(-\tau) = \frac{M\phi(0) - g_2(0)}{\lambda - N} e^{\lambda\tau} - \int_0^\tau e^{-\lambda(\tau+\xi)} g_2(\xi)\mathrm{d}\xi. \tag{37}$$

Substituting (37) into the first Eq. of (27), from Lemma 2.1 and (35), we have

$$\begin{aligned}(f_{u_*} - \lambda)\phi(0) =& g_1(0) - d_1(\phi(0))_{xx} - d_2 u_* e^{-\lambda\tau}(K * (\frac{M\phi(0) - g_2(0)}{\lambda - N}))_{xx} \\ & - d_2 u_* (K * (q(-\tau)))_{xx} \\ =& g_1(0) - d_1(\phi(0))_{xx} - d_2 u_* e^{-\lambda\tau} \frac{M}{\lambda - N}(K * (\phi(0))_{xx}) \\ & - d_2 K * (q(-\tau))_{xx}. \end{aligned} \tag{38}$$

Taking the inner products with both sides of (38) and ψ_n and then combining (8) and (35) give that

$$\begin{aligned}(f_{u_*} - \lambda)c_n(\phi(0)) =& c_n(g_1(0)) + (d_1 + d_2 u_* e^{-\lambda\tau} \frac{M}{\lambda - N} H(n, R))l_n c_n(\phi(0)) \\ & - c_n(q(-\tau))H(n, R). \end{aligned} \tag{39}$$

Therefore, for $\lambda \in \mathbb{C}\backslash\{\lambda_n, n \in \mathbb{Z}\}$, it is clear that $\lambda - \lambda_n \neq 0$. Since $E(n, \tau, \lambda) = 0$ is given in (20) and (21), we have

$$c_n(\phi(0)) = \frac{-c_n(g_1(0)) + c_n(q(-\tau))H(n, R)}{\lambda - \lambda_n}.$$

Letting $\phi(0) = \Sigma_{n\in\mathbb{Z}} c_n(\phi(0))\psi_n(x)$ and $\varphi(0) = \frac{M\phi(0)-g_2(0)}{\lambda-N}$, then (22) has a unique solution $\Phi(\theta)$ defined in (24) for $\lambda \in \mathbb{C}\backslash\{\lambda_n, n \in \mathbb{Z}\}$, which implies that $\lambda \in \mathbb{C}\backslash\{\lambda_n, n \in \mathbb{Z}\} \subset \mathbb{C}\backslash\sigma(\mathcal{L})$, that is, $\sigma_p(\mathcal{L}) \subset \sigma(\mathcal{L})$. The proof is completed. □

Remark 2.4 Since $N = -(\mu + \beta u_*) < 0$, the stability of the positive steady state (u_*, w_*) to (4) is determined by the distribution of roots to the characteristic equation $E(n, \tau, \lambda) = 0$.

3 Stability and Turing Instability

We first consider system (4) without the nonlocal advection term, i.e, $d_2 = 0$. The Jacobian matrix $\mathcal{L}_0$ at the positive steady state (u_*, w_*) is given in (14). Then, we have the trace $\mathrm{Tr}(\mathcal{L}) = f_{u_*} + N < 0$, and the determinant $\mathrm{Det}(\mathcal{L}) = f_{u_*}N > 0$, which means that the positive steady state (u_*, w_*) is linearly asymptotically stable. In the following, we investigate the system (4) with $d_2 \neq 0$.

When $\tau = 0$, the characteristic equation of the positive steady state (u_*, w_*) is

$$E_0(n, \lambda) = \lambda^2 + (d_1 l_n - f_{u_*} - N)\lambda + f_{u_*}N - (d_1 N - d_2 u_* M H(n, R))l_n. \quad (40)$$

since $d_1 l_n - f_{u_*} - N > 0$ for any $n \in \mathbb{N}$, then the sign of the real part of the roots to the characteristic Eq. (40) is determined by the sign of $(f_{u_*}N - (d_1 N - d_2 u_* M H(n, R))l_n)$, which depends on the sign of $H(n, R)$. It follows from (15) that for the different kernel functions of (4) and $n \in \mathbb{N}$, the different Fourier coefficients could be calculated in the following forms:

$$\text{Gaussian:} \quad H(n, R) = e^{-\frac{R^2 n^2 \pi^2}{2L^2}} > 0, \quad (41)$$

$$\text{Laplacian:} \quad H(n, R) = \frac{1}{1 + R^2 n^2 \pi^2 / L^2} > 0, \quad (42)$$

$$\text{Top-hat:} \quad H(n, R) = \begin{cases} \dfrac{\sin(n\pi R/L)}{n\pi R/L}, & n \neq 0, \\ 1, & n = 0. \end{cases} \quad (43)$$

For the Gaussian and Laplacian kernel functions, there is $H(n, R) > 0$, and then, $(f_{u_*}N - (d_1 N - d_2 u_* M H(n, R))l_n) > 0$ for $n \in \mathbb{N}$. According to the Routh–Hurwitz theory, we have the following results.

Theorem 3.1 *Under the assumption* $(\mathbf{H_0})$*, when the nonlocal memory kernel is selected to a Gaussian or Laplacian kernel function, the positive steady state* (u_*, w_*) *of* (4) *is linearly asymptotically stable for any* $R \geq 0$ *and* $\tau = 0$*.*

Then, we focus on the Top-hat kernel function since the sign of $H(n, R)$ defined in (43) is variable. To investigate the influence of perceptual range R on the stability of positive steady state (u_*, w_*), we consider the following equation:

$$\frac{\sin n\pi R/L}{n\pi R/L} = \frac{d_1 N}{d_2 u_* M} - \frac{f_{u_*}N}{d_2 u_* M l_n}, \quad (44)$$

Let $H(n, R) = \frac{\sin(n\pi R/L)}{n\pi R/L}$, it follows from Proposition 3.3 of Xue et al. (2024) and Proposition 3.1 of Song et al. (2024) that $H(n, R)$ have the local extremum at $n = n_j^R$, $(j = 0, 1, 2, \dots)$ for fixed R, where n_j^R are solutions of $H'(n, R) = 0$, i.e.,

$$\tan(n\pi R/L) = n\pi R/L, \quad (45)$$

with $0 < n_j^R < n_{j+1}^R$. One can easily obtain that

$$|H(n_{j+1}^R, R)| < |H(n_j^R, R)| < 1.$$

Moreover, the local extremum of $H(n, R)$ is independent of R. Denote $z_j = H(n_j^R, R)$, it is clear that $H(n, R)$ attains a local minimum $z_{2m-1} < z_{2m+1} < 0$ when $j = 2(m-1)+1$ is odd, and a local maximum $z_{2m} > z_{2m+2} > 0$ when $j = 2m$ is even, where $m \in \mathbb{N}^+$. On the other hand, when R is increasing, we have

$$\lim_{R\to 0} n_j^R = +\infty, \quad \lim_{R\to\infty} n_j^R = 0.$$

For simple calculations, we denote

$$S := S(p, \mu, \beta) = -\frac{N}{u_* M} = \frac{(\mu + \beta u_*)^2}{p u_*^2 (2\mu + \beta u_*)},$$

it is clear that the partial derivatives of S for p, μ and β are

$$\begin{aligned} S_p &= -\frac{(\mu + \beta u_*)^2}{p^2 u_*^2 (2\mu + \beta u_*)} < 0, \quad S_\mu = \frac{2\mu(\mu + \beta u_*)}{p u_*^2 (2\mu + \beta u_*)^2} > 0, \\ S_\beta &= \frac{(\mu + \beta u_*)(3\mu + \beta u_*)}{p u_* (2\mu + \beta u_*)^2} > 0. \end{aligned} \tag{46}$$

The following results on the distribution of roots to Eq. (44).

Lemma 3.2 *Under the assumption* ($\mathbf{H_0}$)*, when the nonlocal memory kernel is selected to the Top-hat kernel function, the following results hold for* $\tau = 0$.

(i) If $d_2 \le -\frac{S}{z_1} d_1$*, then Eq.* (44) *has no roots;*

(ii) If $-\frac{S}{z_{2m-1}} d_1 < d_2 < -\frac{S}{z_{2m+1}} d_1$, $(m = 1, 2, \dots)$*, there exists a threshold* $R = R_*$*, where* $R_* = \max\{R_1, R_2, \cdots R_i\}$, $i = 1, 2, \cdots m$*, and* R_i *satisfies*

$$H(n_{2m-1}^{R_i}, R_i) = F(n_{2m-1}^{R_i}), \tag{47}$$

such that when $R > R_*$*, Eq.* (44) *has no roots; when* $R < R_*$*, Eq.* (44) *has at least two roots; when* $R = R_*$*, Eq.* (44) *has only one root* $(n_*, F(n_*))$.

Proof We firstly focus on the right side of Eq. (44) and denote

$$F(n) = \frac{d_1 N}{d_2 u_* M} - \frac{f_{u_*} N}{d_2 u_* M l_n}, \tag{48}$$

where $l_n = (\frac{n\pi}{L})^2$. Solving the roots of Eq. (44) is equivalent to finding the intersection of curves $H(n, R)$ and $F(n)$. One can easily check that $F(n)$ monotonically increases

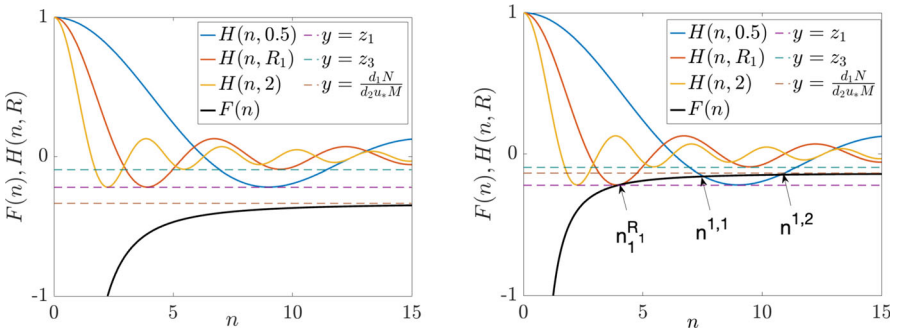

Fig. 3 The graph of $F(n)$ and $H(n, R)$ for $R < R_1$, $R = R_1$, and $R > R_1$ when m=1

for n, which is independent of R. Additionally, we have

$$\lim_{n\to 0^+} F(n) = -\infty, \quad \lim_{n\to\infty} F(n) = \frac{d_1 N}{d_2 u_* M} < 0,$$

since $N < 0$ and $M > 0$, which means that

$$F(n) < \frac{d_1 N}{d_2 u_* M} < 0, \quad n \in \mathbb{N}^+.$$

From the above discussion on the local extremum of $H(n, R)$, we know that $H(n, R)$ attains the minimum at $n = n_1^R$ with

$$\min_{n>0,R>0} H(n, R) = z_1 = \frac{\sin n_1^R \pi R/L}{n_1^R \pi R/L} < 0.$$

Obviously, when $d_2 \le -\frac{S}{z_1} d_1$, we have $F(n) < \min_{n>0,R>0} H(n, R)$. there is no intersection of curves $H(n, R)$ and $F(n)$. This completes the proof of (i) (Fig. 3).

When $m = 1$, there is $-z_1 S d_1 < d_2 < -z_3 S d_1$, which implies that

$$z_1 < \frac{d_1 N}{d_2 u_* M} < z_3.$$

There exists a threshold $R = R_1$, such that

$$H(n_1^{R_1}, R_1) = F(n_1^{R_1}).$$

That means, when $R = R_1$, the curves $H(n, R)$ and $F(n)$ are tangent at $n = n_1^{R_1}$; when $R > R_1$, there is still no intersection of curves $H(n, R)$ and $F(n)$; when $R < R_1$, there are two intersections $n = n^{1,1} \in (0, n_1^R)$ and $n = n^{1,2} \in (n_1^R, n_2^R)$, shown in Fig. (3).

When $m > 1$, similar to the proof of $m = 1$, for $-\frac{S}{z_{2m-1}}d_1 < d_2 < -\frac{S}{z_{2m+1}}d_1$, there exists a threshold $R = R_m$, such that the curves $H(n, R)$ and $F(n)$ are tangent at $n = n^{R_m}_{2m-1}$, and (47) holds. When $R > R_m$, there is no intersection; when $R < R_m$, there are at least two intersections $n = n^{m,1} \in (n^R_{2m-2}, n^R_{2m-1})$ and $n = n^{m,2} \in (n^R_{2m-1}, n^R_{2m})$ and at most $2i$. The proof is completed. □

Then we have the following theorem.

Theorem 3.3 *Under the assumption* ($\mathbf{H_0}$)*, when the nonlocal memory kernel is selected to the Top-hat kernel function, and* $\tau = 0$*, the following results hold.*

(i) If $d_2 \le -\frac{S}{z_1}d_1$*, then the positive steady state* (u_*, w_*) *of* (4) *is linearly asymptotically stable for any* $R > 0$*;*

(ii) If $d_2 > -\frac{S}{z_1}d_1$*, then there exists a threshold* $R = R_*$*, such that when* $R > R_*$*, the positive steady state* (u_*, w_*) *is linearly asymptotically stable and unstable for* $0 < R < R_*$*. Moreover, the system* (4) *has a stationary Turing crossing when* $R = R_*$*.*

Proof From Lemma 3.2, when $d_2 \le -\frac{S}{z_1}d_1$, Eq. (44) has no roots, that is, $H(n, R) > F(n)$, i.e., $(f_{u_*}N - (d_1N - d_2u_*MH(n, R))l_n) > 0$, which means that all of the eigenvalues of the characteristic Eq. (40) have negative real parts. Moreover, when $d_2 > -\frac{S}{z_1}d_1$, Eq. (44) has at least two roots $n = n^{m,1} \in (n^R_{2m-2}, n^R_{2m-1})$ and $n = n^{m,2} \in (n^R_{2m-1}, n^R_{2m})$; then, $H(n, R) < F(n)$ for $n^{m,1} < n < n^{m,2}$, which means that $(f_{u_*}N - (d_1N - d_2u_*MH(n, R))l_n) < 0$. That is, there exists a $n = n_\epsilon \in \mathbb{N}$, such that the characteristic Eq. (40) has an eigenvalue with a positive real part. The proof is completed. □

Remark 3.4 When the nonlocal perception kernel is a Top-hat kernel function, Liu et al. (2025) studied the Turing bifurcation of (4) caused by the nonlocal perception coefficient d_2 for $\tau = 0$. However, we investigate the Turing bifurcation at the positive steady state (u_*, w_*) of (4) caused by the perceptual radius R.

There is an insight that comes from the role of the perception kernel. For smooth kernels such as Gaussian or Laplacian, the positive steady state remains linearly asymptotically stable when $\tau = 0$, indicating that gradual, distance-weighted perception tends to suppress spatial overreaction. In contrast, the Top-hat kernel, which has a sharp spatial cut-off, allows abrupt changes in perceived conflict intensity, enabling the amplification of local perturbations and the emergence of Turing instabilities. Ecologically, this highlights that not only the strength of memory but also the manner in which individuals integrate spatial information can qualitatively alter population-level outcomes: smooth perception promotes stability, whereas sharply localized perception facilitates segregation patterns.

On the other hand, it is worth noting that spatial pattern formation arises from the interaction between cognition-driven avoidance and the perceptual scale. When

memory-based movement is weak, random dispersal dominates and prevents spatial structuring. Once memory effects become sufficiently strong, individuals intensively avoid previously contested sites, and pattern formation becomes possible if perception is limited to a small neighborhood. A larger perception radius counteracts this tendency by smoothing conflict information. The dependence of S on (p, μ, β) further clarifies this mechanism: frequent or intense conflicts (larger p) reduce the stability region and promote instability, whereas faster decay or resetting of conflict memory (larger μ or β) enlarge the stability region and thus suppress pattern formation. Ecologically, this indicates that populations with persistent conflict memory and localized perception are more prone to spatial segregation, whereas those that forget or reassess past conflicts maintain more homogeneous spatial distributions.

4 Hopf Crossings and Turing-Hopf Spectral Thresholds

In this section, we investigate the influence of the memory delay $\tau > 0$, and the perceptual radius $R > 0$ on the stability of the positive steady state (u_*, w_*) to (4). For this purpose, we first study the distribution of the purely imaginary eigenvalues of (20) for $\tau > 0$.

Letting $\lambda_n = i\omega_n$, $(\omega_n > 0)$ be the purely imaginary eigenvalues of (20), substituting $\lambda_n = i\omega_n$ into the characteristic Eq. (20), and then separating the real and imaginary parts yields

$$\begin{cases} Q_n \cos(\omega_n \tau) = \omega_n^2 - P_n, \\ Q_n \sin(\omega_n \tau) = B_n \omega_n, \end{cases} \tag{49}$$

where B_n, P_n, and Q_n are defined in (21). It is easy to obtain that

$$Q_n^2 = (\omega_n^2 - P_n)^2 + B_n^2 \omega_n^2,$$

which means that $y_n = \omega_n^2$ is a solution of the following equation:

$$y_n^2 + (B_n^2 - 2P_n) y_n + P_n^2 - Q_n^2 = 0, \tag{50}$$

we have

$$y_n = \frac{1}{2}((2P_n - B_n^2) \pm \sqrt{(B_n^2 - 2P_n)^2 - 4(P_n^2 - Q_n^2)}), \tag{51}$$

where

$$\begin{aligned} B_n^2 - 2P_n =& d_1^2 l_n^2 - 2d_1 f_{u_*} l_n + (f_{u_*}^2 + N^2) > 0, \\ P_n^2 - Q_n^2 =& [f_{u_*} N - d_1 N l_n + d_2 u_* M H(n, R) l_n][f_{u_*} N - d_1 N l_n - d_2 u_* M H(n, R) l_n]. \end{aligned} \tag{52}$$

Hence, the existence of ω_n is determined by the sign of $(P_n^2 - Q_n^2)$, which is discussed for the different nonlocal perception kernels in the following.

4.1 Gaussian and Laplacian Kernel Cases

When the nonlocal perception kernel is chosen to be a Gaussian or Laplacian kernel function, both of the Fourier coefficients defined in (41) and (42) are positive, which means that $(f_{u_*}N - d_1 N l_n + d_2 u_* M H(n, R) l_n) > 0$. Denote

$$G(n) = -\frac{d_1 N}{d_2 u_* M} + \frac{f_{u_*} N}{d_2 u_* M l_n}, \tag{53}$$

where $l_n = (\frac{n\pi}{L})^2$. It is easy to see that $G(n)$ is independent of R and monotonically decreases for n, we have

$$\lim_{n\to 0^+} G(n) = +\infty, \quad \lim_{n\to\infty} G(n) = -\frac{d_1 N}{d_2 u_* M} > 0,$$

which means that

$$G(n) > -\frac{d_1 N}{d_2 u_* M} > 0, \quad n \in \mathbb{N}^+.$$

Firstly, we consider the Gaussian kernel functions, let

$$H(n, R) = e^{-\frac{R^2 n^2 \pi^2}{2L^2}}, \tag{54}$$

we have $0 < H(n, R) < 1$, $H(n, R)$ is decreasing for n and R. Similar to the discussion in Lemma (3.2), the following result is obtained.

Lemma 4.1 *Under the assumption* $(\mathbf{H_0})$*, when the nonlocal memory kernel is selected to be the Gaussian kernel function, we have the following results for* $\tau > 0$*:*

(i) If $d_2 \le Sd_1$*, then there are no purely imaginary eigenvalues of* (20)*;*
(ii) If $d_2 > Sd_1$*, then there exists a threshold* $R_H > 0$*, which depends on* d_1 *and* d_2*, such that when* $R \ge R_H$*, the characteristic Eq.* (20) *has no purely imaginary eigenvalues; When* $0 < R < R_H$*, curves* $H(n, R)$ *and* $G(n)$ *have two intersections* $n_G^{(1)}$ *and* $n_G^{(2)}$*, such that* (20) *has a purely imaginary eigenvalue for* $n \in (n_G^{(1)}, n_G^{(2)})$ *and no purely imaginary eigenvalues for* $n \in (0, n_G^{(1)}) \cup (n_G^{(2)}, +\infty)$*.*

Proof Obviously, when $d_2 \le Sd_1$, there is $G(n) > 1 \ge H(n, R)$, which implies that $P_n^2 - Q_n^2 > 0$, and (50) have no positive roots for $n \in \mathbb{N}^+$, this completes the proof of (i). When $d_2 > Sd_1$, there is $-\frac{d_1 N}{d_2 u_* M} < 1$. It follows from the properties of $H(n, R)$ and $G(n)$ that there exists a threshold $R_H > 0$, such that curves $H(n, R)$ and $G(n)$ are tangent at $n_G^{R_H}$, shown in Fig. 4.

When $R > R_H$, we have $G(n) > H(n, R)$, which means that $P_n^2 - Q_n^2 > 0$, (50) have no positive roots for $n \in \mathbb{N}^+$; when $0 < R < R_H$, curves $H(n, R)$ and $G(n)$ have two intersections $n_G^{(1)} \in (0, n_G^{R_H})$ and $n_G^{(2)} \in (n_G^{R_H}, +\infty)$. We have $G(n) < H(n, R)$ for $n \in (n_G^{(1)}, n_G^{(2)})$, and $G(n) > H(n, R)$ for $n \in (0, n_G^{(1)}) \cup (n_G^{(2)}, +\infty)$. The proof is completed. □

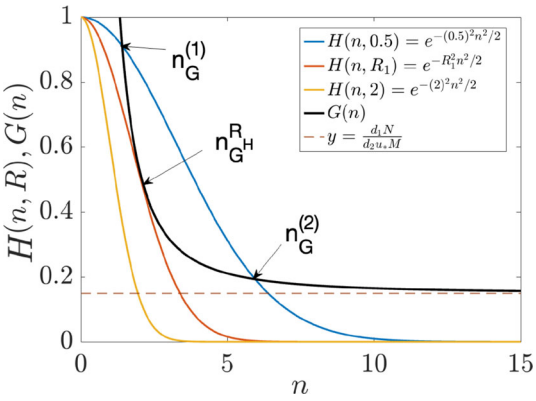

Fig. 4 The graph of $G(n)$ and $H(n, R)$ for $R < R_H$, $R = R_H$, and $R > R_H$

Under the assumptions $d_2 > Sd_1$ and $0 < R < R_H$. It follows from the second Eq. of (49), $B_n > 0$, and $Q_n > 0$ that $\sin \omega_n \tau > 0$, and there exists a pair of purely imaginary eigenvalues $\pm i\omega_n$ at $\tau = \tau_n^j$, $j \in \mathbb{N}_0$, $n \in (n_G^{(1)}, n_G^{(2)})$, where $\omega_n = \sqrt{y_n}$, y_n is defined in (51), and

$$\tau_n^j = \frac{1}{\omega_n}\{\arccos\frac{\omega_n^2 - P_n}{Q_n} + 2j\pi\}, \quad j \in \mathbb{N}_0, \quad n \in (n_G^{(1)}, n_G^{(2)}). \tag{55}$$

To verify the Hopf transversality condition at the spectral crossing, we give the following lemma.

Lemma 4.2 *Under the assumptions* $(\mathbf{H_0})$ *and* $d_2 > Sd_1$, *the following transversality conditions hold:*

$$\mathrm{Re}(\frac{\mathrm{d}\lambda(\tau)}{\mathrm{d}\tau})|_{\tau=\tau_n^j} > 0. \tag{56}$$

Proof Differentiating with respect to τ on both sides of the characteristic Eq. (20) yields

$$\frac{\mathrm{d}\lambda_n}{\mathrm{d}\tau} = \frac{\lambda_n Q_n}{(2\lambda_n + B_n)e^{\lambda_n \tau} - \tau Q_n}, \tag{57}$$

substituting $\lambda_n = i\omega_n$ into (57), and separating the real part, we have

$$\begin{aligned}\frac{\mathrm{d}\lambda_n}{\mathrm{d}\tau} =& \frac{i\omega_n Q_n}{(2i\omega_n + B_n)e^{i\omega_n\tau} - \tau Q_n}\\ =& \frac{i\omega_n Q_n}{(B_n\cos\omega_n\tau - 2\omega_n\sin\omega_n\tau - \tau Q_n) + i(2\omega_n\cos\omega_n\tau + B_n\sin\omega_n\tau)}\\ =& \frac{\omega_n Q_n(2\omega_n\cos\omega_n\tau + B_n\sin\omega_n\tau) + i\omega_n Q_n(B_n\cos\omega_n\tau - 2\omega_n\sin\omega_n\tau - \tau Q_n)}{(B_n\cos\omega_n\tau - 2\omega_n\sin\omega_n\tau - \tau Q_n)^2 + (2\omega_n\cos\omega_n\tau + B_n\sin\omega_n\tau)^2},\end{aligned}$$

combining (49) and (55), there is

$$\omega_n Q_n(2\omega_n\cos\omega_n\tau + B_n\sin\omega_n\tau) = 2\omega_n^4 + (B_n^2 - 2P_n)\omega_n^2 > 0,$$

which implies that (56) holds. The proof is completed. □

Combining Lemma 4.1 and Lemma 4.2, we obtain the following results for $\tau \geq 0$ and $R \geq 0$.

Theorem 4.3 *Under the assumption* $(\mathbf{H_0})$*, we have the following results:*

(i) If $d_2 \leq Sd_1$*, then the positive steady state* (u_*, w_*) *of* (4) *is linearly asymptotically stable for any* $\tau \geq 0$ *and* $R \geq 0$.

(ii) If $d_2 > Sd_1$*, then there exists a threshold* $R_H > 0$*, such that when* $R \geq R_H$*,* (u_*, w_*) *of* (4) *is linearly asymptotically stable for any* $\tau \geq 0$*; when* $0 < R < R_H$*, there exists a critical value* τ_G^**, such that* (u_*, w_*) *is linearly asymptotically stable for* $\tau \in [0, \tau_G^*)$*,* (u_*, w_*) *is unstable for any* $\tau \in (\tau_G^*, +\infty)$*, and the system* (4) *has a Hopf crossing at* $\tau = \tau_G^*$.

Remark 4.4 Since the Fourier coefficient of the Laplacian kernel function has similar properties to those of the Gaussian kernel, the Laplacian kernel case has the same results as Lemmas 4.1, 4.2, and Theorem 4.3.

4.2 Top-Hat Kernel Case

In the following, we consider the case for the Top-hat kernel function. Similar to the discussion of the Gaussian kernel case, we have the following results:

Lemma 4.5 *Under the assumption* $(\mathbf{H_0})$*, when the nonlocal memory kernel is selected to be the Top-hat kernel function, the following results hold for* $\tau > 0$*:*

(i) If $d_2 \leq Sd_1$*, then there are no purely imaginary eigenvalues of the characteristic Eq.* (20)*;*

(ii) If $Sd_1 < d_2 \leq -\dfrac{S}{z_1}d_1$*, there exists a threshold* $R_*^H > 0$*, such that when* $R \geq R_*^H$*, Eq.* (20) *has no purely imaginary eigenvalues; when* $0 < R < R_*^H$*, there exists* $n_H^{(1)}$ *and* $n_H^{(2)}$*, such that* (20) *has a pair of purely imaginary eigenvalues* $\pm i\omega_n$ *for* $n \in (n_H^{(1)}, n_H^{(2)})$ *and no purely imaginary eigenvalues for* $n \in (0, n_H^{(1)}) \cup (n_H^{(2)}, +\infty)$*, where* $\omega_n = \sqrt{y_n}$*,* y_n *is defined in* (51)*, and*

$$\tau_n^j = \frac{1}{\omega_n}\{\arccos\frac{\omega_n^2 - P_n}{Q_n} + 2j\pi\}, \quad j \in \mathbb{N}_0, \quad n \in (n_H^{(1)}, n_H^{(2)}). \tag{58}$$

(iii) If $-\dfrac{S}{z_{2m-1}}d_1 < d_2 \leq \dfrac{S}{z_{2m}}d_1$*,* $(m = 1, 2, \ldots)$*, there is* $R_*^H > R_*$*, such that when* $R > R_*^H$*,* (20) *has no purely imaginary eigenvalues, where* R_* *is defined in Lemma 3.2; when* $R_* < R < R_*^H$*,* (20) *has a pair of purely imaginary eigenvalues* $\pm i\omega_n$ *for* $n \in (n_H^{(1)}, n_H^{(2)})$ *and* τ_n^j *defined by* (58)*, and no purely imaginary eigenvalues for* $n \in (0, n_H^{(1)}) \cup (n_H^{(2)}, +\infty)$.

(iv) If $\dfrac{S}{z_{2m}}d_1 < d_2 \leq -\dfrac{S}{z_{2m+1}}d_1$*,* $(m = 1, 2, \ldots)$*, there is* $R_*^H < R_*$*, such that when* $R > R_*$*,* (20) *has no purely imaginary eigenvalues.*

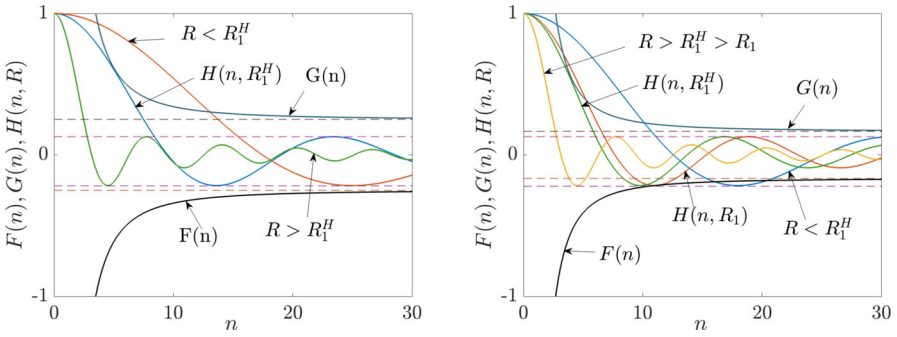

Fig. 5 The graph of $F(n)$, $G(n)$ and $H(n, R)$ for $R < R_1^H$, $R = R_1^H$, $R = R_1$, and $R > R_1$ when $m = 1$

Proof Similar to the proof of Lemma 4.1, together with Theorem 3.3, immediately yields (i) and (ii), we omit it and only prove (iii) and (iv) here.

When $m = 1$, there is

$$\frac{d_1 N}{d_2 u_* M} > z_1, \quad \text{and} \quad -\frac{d_1 N}{d_2 u_* M} > z_2,$$

it follows from the properties of $H(n, R)$ and $G(n)$ that there exists a threshold $R_1^H > R_1 > 0$, such that curves $H(n, R)$ and $G(n)$ are tangent at $n_H^{R_1^H}$. Combining Theorem (3.3), we have $G(n) > H(n, R) > F(n)$ for $R > R_1^H$, which implies that $P_n^2 - Q_n^2 > 0$. When $R_1 < R < R_1^H$, we have $H(n, R) > F(n)$ for $n > 0$, $H(n, R) > G(n)$ for $n \in (n_R^{1,1}, n_R^{1,2})$, and $H(n, R) < G(n)$ for $n \in (0, n_R^{1,1}) \cup (n_R^{1,2}, +\infty)$, where $n_R^{1,1}$ and $n_R^{1,2}$ are two intersections of curves $H(n, R)$ and $G(n)$, as shown in Fig. 5.

When $m > 1$, letting

$$R_*^H = \max\{R_1^H, R_3^H, \ldots, R_{2m-1}^H\}, \quad R_* = \max\{R_1, R_3, \ldots, R_{2m-1}\},$$

where R_{2m-1} is defined in (48), and R_{2m-1}^H satisfies

$$H(n_H^{R_{2m-1}^H}, R_{2m-1}^H) = G(n_H^{R_{2m-1}^H}),$$

and $0 < R_{2m-1} < R_{2m-1}^H$. Similar to the proof of $m = 1$, it is easy to confirm (iii).

One can easily check that $R_{2m-1} > R_{2m-1}^H$ when $\frac{S}{z_{2m}} d_1 < d_2 \le -\frac{S}{z_{2m+1}} d_1$. By a similar discussion of (iii), we could confirm (iv). □

Lemma 4.6 *Under the assumption* ($\mathbf{H_0}$)*, the following transversality conditions hold:*

$$\mathrm{Re}\left(\frac{\mathrm{d}\lambda(\tau)}{\mathrm{d}\tau}\right)\Big|_{\tau=\tau_n^j} > 0. \tag{59}$$

and, at a simple Turing threshold $R = R_*$ associated with the mode $n = n_*$,

$$\frac{\mathrm{d}\lambda(R)}{\mathrm{d}R}|_{R=R_*,n=n_*} < 0. \tag{60}$$

Proof We only prove (60), differentiating with respect to R on both sides of the characteristic Eq. (20) yields

$$\frac{\mathrm{d}\lambda(R)}{\mathrm{d}R} = -\frac{d_2 u_* M H_R(n, R) l_n e^{-\lambda\tau}}{2\lambda + B_n - \tau Q_n e^{-\lambda\tau}}.$$

At the Turing threshold, $\lambda = 0$ and $P_n + Q_n = 0$. Therefore,

$$\left.\frac{d\lambda}{dR}\right|_{R=R_*,\, n=n_*} = -\frac{d_2 u_* M H_R(n_*, R_*) l_{n_*}}{B_{n_*} + \tau P_{n_*}}. \tag{61}$$

For the Top-hat kernel, there is $H(n, R) = \frac{\sin(k_n R)}{k_n R}$ with $k_n = \frac{n\pi}{L}$, and hence we have the derivative of $H(n, R)$ with respect to R

$$H_R(n, R) = \frac{k_n R\cos(k_n R) - \sin(k_n R)}{k_n R^2}.$$

Since the first Turing threshold satisfied $\pi < k_{n_*} R_* < \frac{3\pi}{2}$, we have $H_R(n_*, R_*) > 0$. It follows from $B_{n_*} + \tau P_{n_*} > 0$ that (60) holds. The proof is completed. □

According to Theorem 3.3, Lemmas 4.5, and 4.6, the following results of Hopf crossing and Turing-Hopf spectral thresholds are given.

Theorem 4.7 *Under the assumption* ($\mathbf{H_0}$)*, the following results hold:*

(i) If $d_2 \le S d_1$, then the positive steady state (u_*, w_*) of (4) is linearly asymptotically stable for all $R > 0$ and $\tau \ge 0$.

(ii) If $S d_1 < d_2 \le -\frac{S}{z_1} d_1$, there exists a threshold $R_*^H > 0$, such that when $R \ge R_*^H$, (u_*, w_*) is linearly asymptotically stable for $\tau \ge 0$; when $0 < R < R_*^H$, there exists a critical value $\tau_* = \min\limits_{n\in(n_H^{(1)}, n_H^{(2)})} \{\tau_n^0\}$, where τ_n^0 is defined in (58), such that (u_*, w_*) is unstable for $\tau \in (\tau_*, +\infty)$ and linearly asymptotically stable for $\tau \in [0, \tau_*)$, and system (4) has a Hopf crossing at $\tau = \tau_*$.

(iii) If $-\frac{S}{z_{2m-1}} d_1 < d_2 \le \frac{S}{z_{2m}} d_1$, $(m = 1, 2, \dots)$, there is $R_*^H > R_*$, such that when $R \ge R_*^H$, (u_*, w_*) is linearly asymptotically stable; when $R_* < R < R_*^H$, there exists a critical value $\tau_* = \min\limits_{n\in(n_H^{(1)}, n_H^{(2)})} \{\tau_n^0\}$, such that (u_*, w_*) is unstable for $\tau \in (\tau_*, +\infty)$ and linearly asymptotically stable for $\tau \in [0, \tau_*)$, the system (4) has a Hopf crossing at $\tau = \tau_*$; when $0 < R < R_*$, (u_*, w_*) is unstable for $\tau \ge 0$. Moreover, the system has a Turing-Hopf spectral point $(R, \tau) = (R_*, \tau_*)$.

(iv) If $\frac{S}{z_{2m}}d_1 < d_2 \leq -\frac{S}{z_{2m+1}}d_1$, $(m = 1, 2, \dots)$, *there is* $R_*^H < R_*$, *such that when* $R > R_*$, (u_*, w_*) *is linearly asymptotically stable for* $\tau \geq 0$*; when* $0 < R < R_*$, (u_*, w_*) *is unstable for* $\tau \geq 0$. *The system* (4) *has a stationary Turing crossing at* $R = R_*$.

5 Numerical Simulations

In this section, we present numerical simulations to illustrate the stability thresholds obtained from the characteristic equations and the corresponding spatial and spatiotemporal dynamics near the positive steady state (u_*, w_*). We choose the following parameters:

(P) $p = 0.6$, $\mu = 0.2$, $\beta = 0.1$, and $L = 10$,

and the logistic growth in the reaction term, we consider the following model:

$$\begin{cases} u_t = d_1 u_{xx} + d_2(u(K * w(x, t-\tau))_x)_x + u(1-u), & x \in \Omega, t > 0, \\ w_t = pu^2 - (\mu + \beta u)w, & x \in \Omega, t > 0, \\ u(-L, t) = u(L, t), \quad u_x(-L, t) = u_x(L, t). \end{cases} \tag{62}$$

There is a positive steady state $(1, 2)$ of (62). We have

$$M = 2pu_* - \beta w_* = 1, \quad N = -(\mu + \beta u_*) = -0.3, \quad f_{u_*} = -1,$$

and

$$F(n) = -\frac{3d_1}{10d_2} - \frac{3}{10d_2 l_n}, \quad G(n) = \frac{3d_1}{10d_2} + \frac{3}{10d_2 l_n}.$$

5.1 Gaussian Kernel

Firstly, we consider the Gaussian kernel case, and the Fourier coefficient of the Gaussian kernel is defined in (41). Fixing $d_1 = 0.1$, it follows from Theorem (4.3) that the positive steady state $(1, 2)$ is linearly asymptotically stable when $d_2 \leq 0.03$ for any $\tau \geq 0$ and $R \geq 0$ (Fig. 6a), and the Hopf crossing at $(1, 2)$ when $d_2 > 0.03$. We choose $d_2 = 2 > 0.03$; then, there exists a threshold $R_H \approx 2.1694$, such that $(1, 2)$ is linearly asymptotically stable for $\tau \geq 0$ when $R \geq R_H$ (Fig. 6b), when $0 < R < R_H$, there exists a critical value $\tau_G^* \approx 3.7537$, such that $(1, 2)$ is linearly asymptotically stable for $\tau \in [0, 3.7537)$ (Fig. 6 (c)) and unstable for $\tau \in (3.7537, +\infty)$ (Fig. 6 (d)).

5.2 Top-Hat Kernel

By the definition of $H(n, R)$ for the Top-hat kernel case in (43), we have

$$z_1 \approx -0.217 < 0, \quad z_2 \approx 0.128 > 0.$$

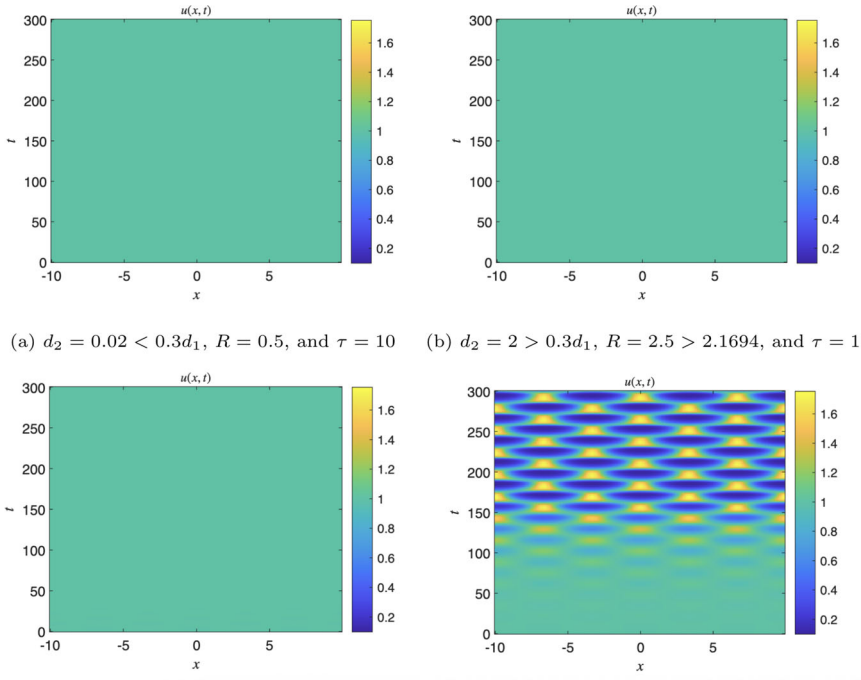

(a) $d_2 = 0.02 < 0.3d_1$, $R = 0.5$, and $\tau = 10$ (b) $d_2 = 2 > 0.3d_1$, $R = 2.5 > 2.1694$, and $\tau = 10$

(c) $d_2 = 2$, $R = 1.5 < 2.1694$, and $\tau = 3 < 3.7537$ (d) $d_2 = 2$, $R = 1.5$, and $\tau = 10 > 3.7537$

Fig. 6 Numerical simulations of (62) for Gaussian kernel case with the initial function $u(x,t) = 1 + 0.01\cos(3\pi x/L)$, $w(x,t) = 2 + 0.01\cos(3\pi x/L)$

5.2.1 Turing Instability for $\tau = 0$

From Theorem (3.3), we choose $d_1 = 0.1$ and have that if $d_2 \leq 1.38d_1$, the positive steady state $(1, 2)$ is linearly asymptotically stable for $R > 0$ and $\tau = 0$ (Fig. 7a). If $d_2 > 1.38d_1$, there exists a threshold $R_* \approx 1.5564$, such that $(1, 2)$ is linearly asymptotically stable for $R > 1.5564$ (Fig. 7b) and unstable for $R < 1.5564$. When R goes through the Turing bifurcation value $R_* \approx 1.5564$ decreasingly, there is a nonconstant steady state for $R < R_*$, and near R_*, we choose $R = 1.5 < 1.5564$ and $R = 1 < 1.5564$; there appears the vertical stripe pattern in Fig. 7 (c) and (d).

5.2.2 Hopf Crossing for $\tau > 0$

It follows from Theorem 4.7(ii) that the Hopf case for the top-hat kernel occurs when $d_2 \in \left(Sd_1, -\frac{S}{z_1}d_1\right] \approx (0.03, 0.138]$. We choose

$$d_1 = 0.1, \qquad d_2 = 0.1 \in (0.03, 0.138].$$

Direct calculation gives $R_H^* \approx 0.5254$. Thus, the positive steady state $(1, 2)$ is linearly asymptotically stable for all $\tau \geq 0$ when $R > 0.5254$. For the particular value $R =$

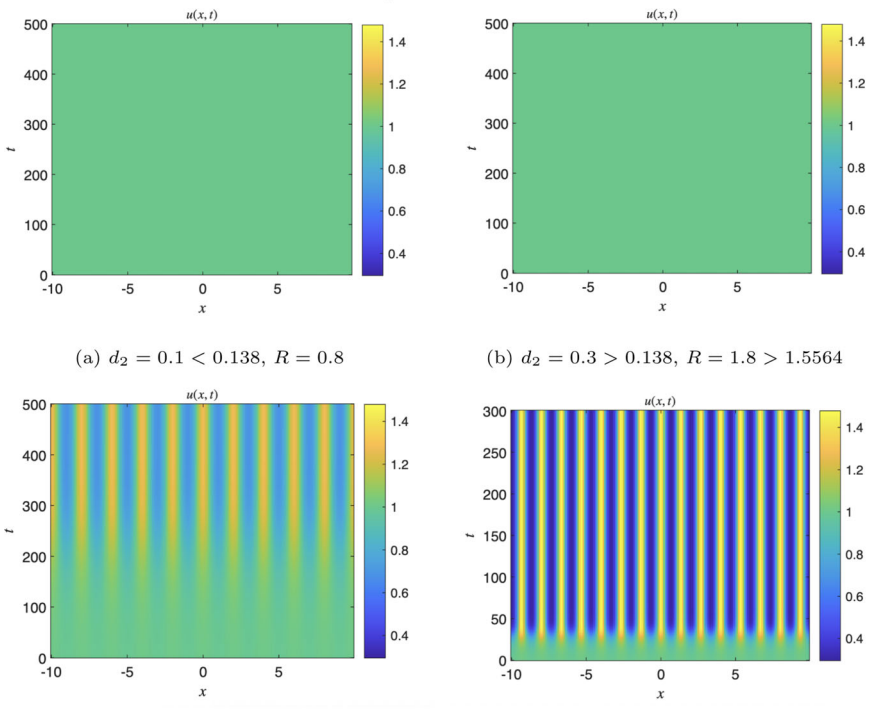

Fig. 7 Numerical simulations of (62) for Top-hat kernel case with $\tau = 0$ and the initial function $u(x,t) = 1 + 0.01\cos(10\pi x/L)$, $w(x,t) = 2 + 0.01\cos(10\pi x/L)$

$0.15 < R_H^*$ used in Fig. 8, the first Hopf threshold is $\tau_*(0.15) \approx 3.1199$. Hence, $(1,2)$ is linearly asymptotically stable for $\tau \in [0, 3.1199)$, as shown in Fig. 8a, while oscillatory instability is observed for $\tau = 4.5 > 3.1199$, as shown in Fig. 8b.

5.2.3 Turing-Hopf Spectral Interaction

From Theorem 4.7(iii), the characteristic equations have both Hopf-crossing thresholds and a Turing-Hopf spectral interaction induced by R and the memory delay τ. We choose $d_1 = 0.1$ and $d_2 = 0.155 \in (1.38d_1, 2.34d_1)$; there are two thresholds $R_* \approx 0.4996$ and $R_*^H \approx 0.7617$ for $n_* = 29$ and $n_H = 10$. By simple calculation, we have the critical value $\tau_* \approx 5.4492$.

For $R \in [0.45, 0.8]$ and $\tau \in [4.5, 12]$, Fig. 9 illustrates the critical spectral-threshold curves, including the Turing threshold line, mode-10 to mode-15 Hopf crossing curves. There is an intersection P_0 of the Turing threshold line and the mode-10 Hopf crossing curves. We choose three different points P_1, P_2, and P_3 to illustrate the spatiotemporal patterns for the Turing-Hopf spectral interaction as follows in Fig. 10.

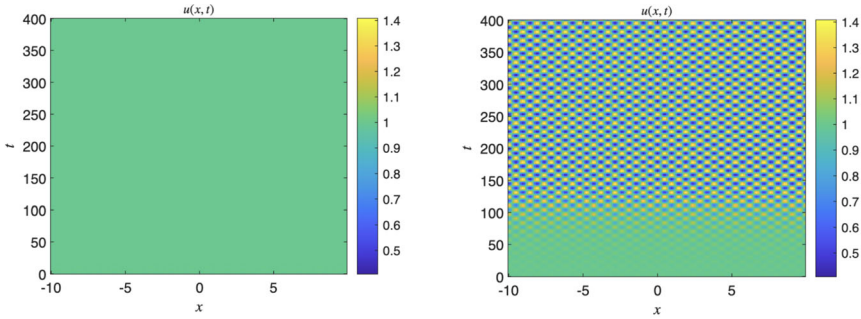

(a) $d_2 = 0.1 \in (0.03, 0.138]$, $R = 0.15 < 0.5254$, and $\tau = 2 < 3.1199$ (b) $d_2 = 0.1$, $R = 0.15$, and $\tau = 4.5 > 3.1199$

Fig. 8 Numerical simulations of (62) for Top-hat kernel with the initial function $u(x,t) = 1 + 0.01\cos(21\pi x/L)$, $w(x,t) = 2 + 0.01\cos(21\pi x/L)$

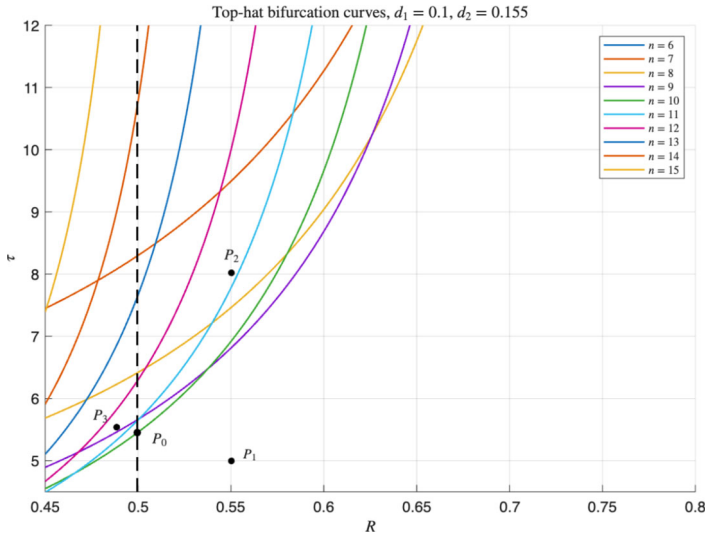

Fig. 9 Spectral threshold curves in plane $R - \tau$ of (62), where $d_1 = 0.1$, $d_2 = 0.155$, the red curve is stationary Turing threshold line $R = R_* = 0.4996$, the curves are mode-10 to mode-15 Hopf crossing curves, respectively. The following numerical simulations of the points, which are chosen by $P_1 = (0.55, 5)$, $P_2 = (0.55, 8)$, and $P_3 = (0.48, 5.5)$

6 Discussion

In this paper, we consider a nonlocal advection model to describe the role of nonlocal spatial memory effects, particularly in response to dynamically evolving conflict zones. Unlike classical diffusive models, we incorporate an ODE to describe the cognitive mapping of high-risk areas. We study the PDE-ODE coupled model (4) and focus on the influence of perceptual radius R and the memory delay τ to the linear stability and spectral thresholds at the positive steady state (u_*, w_*). In biological significance,

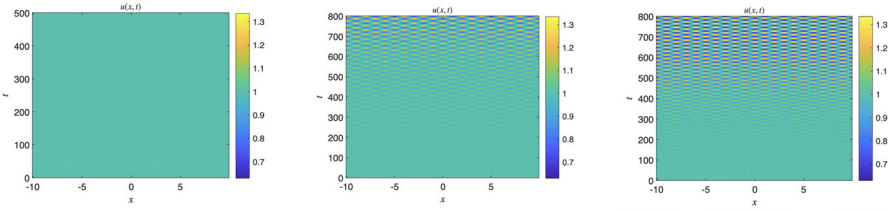

(a) $P_1 = (0.55, 5)$ (b) $P_2 = (0.55, 8)$ (c) $P_3 = (0.48, 5.5)$

Fig. 10 Numerical simulations of P_1, P_2, and P_3 in Fig. 9 with the initial function $u(x,t) = 1 + 0.01\cos(29\pi x/L)$, $w(x,t) = 2 + 0.01\cos(29\pi x/L)$

animals tend to avoid high-risk areas, which is why we consider $d_2 > 0$ in this paper. Additionally, we analyze the spectral properties of the linearized operator, which play a crucial role in determining stability and bifurcation behavior. Our main results include the following.

We consider three types of perceptual kernels, including Gaussian, Laplacian, and Top-hat functions, each representing different ways in which individuals process spatial information. The Gaussian kernel models smooth, long-range perception with a gradual decay in sensitivity, while the Laplacian kernel captures exponentially decreasing perception strength. In contrast, the Top-hat kernel describes a localized, uniform perception range, beyond which no environmental information is retained. Our analysis shows that the choice of kernel affects the system's stability and pattern formation.

For the memoryless case, i.e., $\tau = 0$, when perception is modeled by a Gaussian or Laplacian kernel, the positive steady state remains linearly asymptotically stable for all $R \geq 0$, meaning that species with such perception strategies maintain a homogeneous distribution, shown in Theorem 3.1. However, under the Top-hat kernel, when $d_2 > -\frac{S}{z_1}d_1$, a critical perceptual range R_* exists, beyond which stability persists but below which the system has a stationary Turing crossing, leading to the emergence of stationary spatial patterns, shown in Theorem 3.3. This suggests that species with sharply localized perception are more prone to self-organized spatial structuring.

For the influence of the memory delay $\tau > 0$, our analysis and numerical simulations show that memory delay may lead to Hopf crossings, regardless of the choice of perceptual kernel. The memory delay $\tau > 0$ enters the characteristic equation through $e^{-\lambda\tau}$. In the parameter regimes identified in Sect. 7, a pair of characteristic roots may cross the imaginary axis at a critical delay. The numerical simulations illustrate the oscillatory dynamics associated with this crossing. For the Top-hat kernel, a stationary spatial mode and an oscillatory mode may become critical at the same point in the (R, τ)-plane, producing a Turing-Hopf spectral interaction. While this phenomenon is observed across all kernel types, the Top-hat kernel introduces additional complexity in the system's dynamical behavior. In particular, due to its sharply localized perception structure, the system exhibits Turing-Hopf interactions between a stationary spatial mode and an oscillatory mode, which are associated, in simulations, with more intricate spatiotemporal patterns.

Moreover, our analysis indicates that the stability of the population distribution is strongly influenced by the parameters governing conflict memory. Specifically, as the

conflict generation rate p increases, the stability region shrinks, suggesting that frequent or intense territorial conflicts heighten the likelihood of spatial pattern formation or temporal oscillations. Conversely, larger values of the natural memory decay rate μ or the conflict resetting rate β expand the stability region, indicating that populations capable of rapidly forgetting past conflicts or reassessing previously contested locations tend to maintain more homogeneous and stable distributions. Biologically, this suggests that persistent conflict memory may be associated, in the simulations, with spatial segregation or oscillatory dynamics, whereas efficient memory resetting and decay tend to stabilize the homogeneous distribution.

Several questions remain open. In particular, a complete well-posedness theory for the nonlinear delayed PDE-ODE system, including existence, uniqueness, regularity, and continuous dependence on initial histories, has not been established. In addition, the nonlinear normal forms associated with the Hopf and Turing-Hopf spectral thresholds are not derived here and will be studied elsewhere. Another natural direction is to extend the present framework to two-species systems, where competition or predator–prey interactions may further enrich the effects of conflict memory.

Acknowledgements The authors sincerely thank the Editor and the anonymous reviewers for their careful reading and constructive comments, which greatly helped improve the clarity and presentation of this manuscript.

Author Contributions H.W. designed and supervised the research. S.L. performed the research. S.L., B.D., and H.W. wrote the initial draft. All authors reviewed and edited the manuscript.

Funding S.L.'s research was partially supported by the "Furong Plan" Postdoctoral Funding of Hunan Province. B.D.'s research was partially supported by the National Natural Science Foundation of China (No. 710 12271525). H.W.'s research was partially supported by the Natural Sciences and Engineering Research 711 Council of Canada (Individual Discovery Grant RGPIN-2025-05734) and a Canada Research Chair.

Data Availability No datasets were generated or analyzed during the current study.

Declarations

Conflict of interest The authors declare no conflict of interest.

References

An, Q., Wang, C., Wang, H.: Analysis of a spatial memory model with nonlocal maturation delay and hostile boundary condition. Discrete and Continuous Dynamical Systems: Series A. 1 40(10) (2020)

Ducrot, A., Fu, X., Magal, P.: Turing and Turing-Hopf bifurcations for a reaction diffusion equation with nonlocal advection. J. Nonlinear Sci. **28**, 1959–97 (2018)

Fagan, W.F., Gurarie, E., Bewick, S., Howard, A., Cantrell, R.S., Cosner, C.: Perceptual ranges, information gathering, and foraging success in dynamic landscapes. Am. Nat. **189**(5), 474–89 (2017)

Fagan, W.F., Lewis, M.A., Auger-Méthé, M., Avgar, T., Benhamou, S., Breed, G., LaDage, L., Schlägel, U.E., Tang, W.W., Papastamatiou, Y.P., Forester, J.: Spatial memory and animal movement. Ecol. Lett. **16**(10), 1316–29 (2013)

Golledge, R.G.: editor. Wayfinding behavior: Cognitive mapping and other spatial processes. JHU press (1999)

Li, S., Dai, B., Wang, H.: Existence and stability of steady states of reaction-diffusion equation with spatiotemporal memory. Appl. Math. Lett. **1**(160), 109323 (2025)

Li, S., Li, Z., Dai, B.: Stability and Hopf bifurcation in a prey-predator model with memory-based diffusion. Discr. Continuous Dyn. Syst.-B. **27**(11), 6885–906 (2022)
Li, S., Wang, H., Li, Z., Dai, B.: Spatiotemporal dynamics of competing species with or without memory under Dirichlet boundary condition. Stud. Appl. Math. **155**(4), e70125 (2025)
Li, S., Yuan, S., Jin, Z., Wang, H.: Double Hopf bifurcation induced by spatial memory in a diffusive predator-prey model with Allee effect and maturation delay of predator. Commun. Nonlinear Sci. Numer. Simul. **1**(132), 107936 (2024)
Liu, D., Jiang, W.: Hopf bifurcation in a memory-based diffusion predator-prey model with spatial heterogeneity. J. Diff. Equ. **15**(397), 377–403 (2024)
Liu, D., Potts, J.R., Salmaniw, Y., Shi, J., Wang, H.: Biological aggregations from spatial memory and nonlocal advection. Physica D **29**, 134682 (2025)
Liu, M., Wang, H., Jiang, W.: Bifurcations and pattern formation in a predator-prey model with memory-based diffusion. J. Diff. Equ. **25**(350), 1–40 (2023)
O'Keefe, J., Nadel, L.: The Hippocampus as a Cognitive Map. Oxford University Press, Oxford (1978)
Potts, J.R., Lewis, M.A.: How memory of direct animal interactions can lead to territorial pattern formation. J. R. Soc. Interface **13**(118), 20160059 (2016)
Liu, G., Wang, H., Zhang, X.: Wellposedness, equilibria, and patterns of an epidemic PDE model with spatiotemporally nonlocal memory. J. Diff. Equ. **15**(442), 113491 (2025)
Shen, H., Song, Y., Wang, H.: Bifurcations in a diffusive resource-consumer model with distributed memory. J. Diff. Equ. **25**(347), 170–211 (2023)
Shi, J., Shi, Q.: Spatial movement with temporally distributed memory and Dirichlet boundary condition. J. Diff. Equ. **25**(389), 305–37 (2024)
Shi, Q., Shi, J., Wang, H.: Spatial movement with distributed memory. J. Math. Biol. **82**(4), 33 (2021)
Shi, Q., Song, Y.: Spatial movement with nonlocal memory. Discr. Continuous Dyn. Syst. B. **28**(11), 5580–96 (2023)
Shi, Q., Song, Y., Wang, H.: Local perception and learning mechanisms in resource-consumer dynamics. SIAM J. Appl. Math. **84**(3), 988–1010 (2024)
Shi, J., Wang, C., Wang, H.: Diffusive spatial movement with memory and maturation delays. Nonlinearity **32**(9), 3188 (2019)
Shi, J., Wang, C., Wang, H.: Spatial movement with diffusion and memory-based self-diffusion and cross-diffusion. J. Diff. Equ. **25**(305), 242–69 (2021)
Shi, J., Wang, C., Wang, H., Yan, X.: Diffusive spatial movement with memory. J. Dyn. Diff. Equat. **32**, 979–1002 (2020)
Song, Y., Wang, H., Wang, J.: Cognitive consumer-resource spatiotemporal dynamics with nonlocal perception. J. Nonlinear Sci **34**(1), 19 (2024)
Song, Y., Wu, S., Wang, H.: Spatiotemporal dynamics in the single population model with memory-based diffusion and nonlocal effect. J. Diff. Equ. **267**(11), 6316–51 (2019)
Turing, A.M.: The chemical basis of morphogenesis. Bull. Math. Biol. **52**(1), 153–97 (1990)
Wang, H., Salmaniw, Y.: Open problems in PDE models for knowledge-based animal movement via nonlocal perception and cognitive mapping. J. Math. Biol. **86**(5), 71 (2023)
Xue, S., Song, Y., Wang, H.: Spatio-temporal dynamics in a reaction-diffusion equation with nonlocal spatial memory. SIAM J. Appl. Dyn. Syst. **23**(1), 641–67 (2024)
Zhang, H., Wang, H., Song, Y., Wei, J.: Diffusive spatial movement with memory in an advective environment. Nonlinearity **36**(9), 4585 (2023)
Zhang, Y., Zhang, X., Li, S.: The effect of self-memory-based diffusion on a predator-prey model. Z. Angew. Math. Phys. **75**(3), 1–8 (2024)
Zollner, P.A.: Comparing the landscape level perceptual abilities of forest sciurids in fragmented agricultural landscapes. Landscape Ecol. **15**, 523–33 (2000)